

Electronic Supplementary Information

Composite formation of covalent organic framework crystals and sugar alcohols for exploring a new class of heat-storage materials

Yoichi Murakami,^{1,2,3,4} Shoma Mitsui,² Shiori Nakagawa,⁵ Xiaohan Wang,²*

Hiroki Fujisawa,⁵ Meguya Ryu,^{5,6,7} and Junko Morikawa^{5,7}*

¹ Laboratory for Zero-Carbon Energy, Institute of Innovative Research, Tokyo Institute of Technology, 2-12-1 Ookayama, Meguro-ku, Tokyo 152-8550, Japan.

² Department of Mechanical Engineering, School of Engineering, Tokyo Institute of Technology, 2-12-1 Ookayama, Meguro-ku, Tokyo 152-8552, Japan.

³ Department of Transdisciplinary Science and Engineering, School of Environment and Society, Tokyo Institute of Technology, 2-12-1 Ookayama, Meguro-ku, Tokyo 152-8552, Japan.

⁴ PRESTO, JST, 4-1-8 Honcho, Kawaguchi, Saitama 332-0012, Japan

⁵ Department of Organic and Polymeric Materials, School of Materials and Chemical Technology, Tokyo Institute of Technology, 2-12-1, Ookayama, Meguro-ku, Tokyo 152-8550, Japan

⁶ National Metrology Institute of Japan, National Institute of Advanced Industrial Science and Technology (AIST), 1-1-1 Umezono, Tsukuba, Ibaraki, 305-8563, Japan.

⁷ CRESTO, JST, 4-1-8 Honcho, Kawaguchi, Saitama 332-0012, Japan

*: Corresponding authors: murakami.y.af@m.titech.ac.jp, morikawa.j.aa@m.titech.ac.jp

List of Contents

S1. Sample preparation

S1.1 Chemicals

S1.2 Growth of COF-300 crystals

S1.3 Post treatments of COF-300 crystals

S1.4 Sample preparation by Method 1 (Fig. S1)

S1.5 Sample preparation by Method 2 (Fig. S2)

S2. Fundamental characterizations of COF-300 crystals

S2.1 Thermogravimetric analysis (TGA) (Fig. S3)

S2.2 Specific heat measurements (Fig. S4)

S2.3 Powder X-ray diffraction (PXRD) analysis (Fig. S5)

S2.4 Fourier-transform infrared (FT-IR) spectroscopy (Fig. S6)

S2.5 Nitrogen adsorption isotherms (Fig. S7)

S3. Single-crystal X-ray diffraction analysis (Figs. S8, S9, S10, Tables S1, S2)

S4. Differential scanning calorimetry (DSC)

S5. Comparison of the molecular size of mannitol and pore size of COF-300 (Fig. S11)

S6. Number of hydrogen-bonded molecules to one Man molecule in crystal (Fig. S12)

S7. Temperature wave analysis (TWA) (Fig. S13)

S8. *In situ* observations of a Man-COF crystal during experiment shown in Fig. 4e (Fig. S14)

References

S1. Sample preparation

S1.1 Chemicals

We purchased tetrakis(4-aminophenyl)methane (TAM) from Accela ChemBio (purity: 95%) and terephthalaldehyde (BDA) from TCI (> 98.0%) to serve as building-block molecules for COF-300 growth. We used 1,4-dioxane from Wako (99.5+%) as the solvent, acetic acid from Wako (99.5+%) as the catalyst, and aniline from Aldrich (\geq 99.5%) as the modulator. We used TAM and BDA without further purification; however, in our COF-300 preparation (Section S1.2), these 1,4-dioxane solutions were passed through a PTFE filter (pore size: 200 nm, Merck-LG, SLLGX13NL) to remove particulate impurities that may affect the COF nucleation.

We purchased the sugar alcohols erythritol (**Eri**) from Wako (> 99.0%) and D-mannitol (**Man**) from TCI (> 99.0%). These SAs were stored in a glovebox (OMNI-LAB, Vacuum Atmospheres Company) until their use; this glovebox is equipped with a circulation gas purifier that maintains the moisture and oxygen concentrations inside the glovebox below 1 ppm.

S1.2 Growth of COF-300 crystals

We grew COF-300 crystals based on the procedures we used previously,^{S1} except without using ionic liquids as a nucleation controller. Typical procedures in this report are as follows. All screw-cap glass vials (capacity: 8, 15, or 20 mL) were first blown with dry nitrogen gas to eliminate particulate matter that may have adhered on the inner wall of the vials. Then, the vials were washed by ultrasonication, first with toluene for 3 min and then with methanol for another 3 min. Subsequently, the vials were dried in an oven at 70 °C before use.

First, two solutions were prepared separately in a screw-cap glass vial. The first solution consisted of 2.5 mL of dioxane, 33.5 mg of BDA, 1.6 mL of acetic acid, and 300 μ L of aniline. The other solution consisted of 2.5 mL of dioxane and 47.6 mg of TAM. After ultrasonication, these solutions were transparent. After each of these solutions was passed through a PTFE filter (pore size: 200 nm; Merck-LG, SLLGX13NL), they were mixed in a new screw-cap glass vial and then stored in the dark at room temperature for

7 days. Typically, we prepared multiple glass vials as one batch so that the necessary amount could be obtained. The crystals grew on the inner wall and bottom of the vials.

S1.3 Post treatments of COF-300 crystals

After 7 days growth of COF-300 crystals, the supernatant was removed using a Pasteur pipette and fresh dioxane was added to remove unreacted TAM, BDA, and aniline as well as acetic acid, all of which dissolved well in dioxane, and then the vial was left for at least one day at room temperature. Subsequently, the solvent was replaced with fresh toluene and then left for more than one day at room temperature. Toluene was used because of its nonpolar nature, which allows the avoidance of surface-tension-induced damage to the pores during the removal of the solvent from COF.^{S2} The crystals were collected from the vials using a Pasteur pipette and placed onto a PTFE membrane filter (T100A025A, ADVANTEC; diameter: 25 mm).

The crystals on the PTFE membrane filter underwent drying with a supercritical CO₂ dryer (JCPD-5, JEOL) and then with our home-built vacuum dryer consisting of a 1" quartz tube and an annular furnace at 120 °C flowing 50 sccm of dry N₂ gas for 3–4 h. Supercritical CO₂ drying was used to minimise the potential risk of the aforementioned surface-tension-induced damage to the pores of COF-300 crystals during removal of the toluene from the crystals. The dried COF-300 crystals were put into screw-cap glass vials and stored in the glovebox until use.

The removal of residual solvents and moisture from COF-300 crystals is important for better loading of SAs, because such residual species can hinder inclusion of SA into the crystals.

S1.4 Sample preparation by Method 1

First, a glass slide was placed on a hotplate (HP130914, Thermo Fisher Scientific), which was placed under a stereomicroscope (SMZ745T, Nikon) equipped with a CMOS camera. Then, COF-300 crystals blended with powdered SA (**Eri** or **Man**) were placed on a glass slide (Fig. S1). The temperature of the hotplate was raised to 15 °C above the melting temperature. Introduction of the transparent droplets of melted SA into COF-300 crystals on a glass slide was monitored with the CMOS camera of the stereomicroscope; we manipulated the crystals so that they contacted the droplets using a thin nickel wire

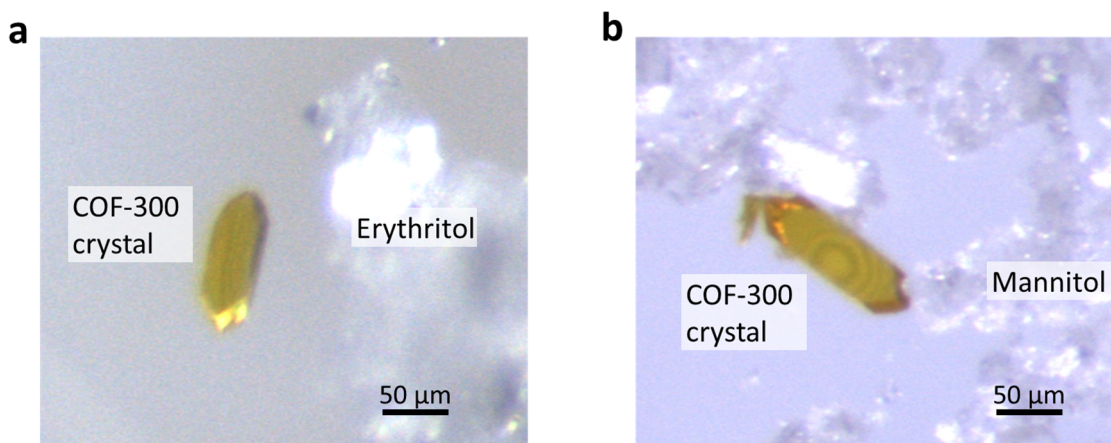


Fig. S1. Typical photographs taken under a stereomicroscope during the process of Method 1 for (a) erythritol and (b) mannitol below their melting temperature.

under the stereomicroscope whenever necessary. Photographs shown in Fig. 2 in the main text were obtained by the CMOS camera during this process.

S1.5 Sample preparation by Method 2

The entire process using this method was conducted in the glovebox, in which O_2 and moisture were controlled below 1 ppm. As mentioned in the main text, all results based on this method are for samples prepared with **Man**.

To introduce the maximum amount of **Man** into COF-300 for a given weight ratio of COF:**Man** in the blended powder and to mitigate the potential effect of dehydration of **Man**, which was reported to occur at elevated temperature,^{S4} we confined a powder blend of COF-300 crystals and **Man** in a tube of paraformaldehyde (PFA; inner diameter: 2 mm; F-8011-002C, FLON INDUSTRY) in which the powder blend was axially compressed by two taper pins made of stainless steel, as indicated by Fig. S2. The weight ratio of COF:**Man** in this study was either 1:0.5 (for Fig. 3b in the main text) or 1:1 (for Figs. 3c, d, and e in the main text). As illustrated in Fig. S2, the tube on a hotplate (RCTBS004, IKA) was covered with a stack of 5 to 7 sheets of aluminium foil as a thermal shield to ensure the uniformity of the temperature between the hotplate face and the aluminium foil above the tube.

During this process, we used a thermocouple enclosed in the PFA tube on the hotplate (Fig. S2) to measure the actual temperature on the hot plate as accurately as possible. We adjusted the hotplate so that this temperature was 170 °C and maintained this temperature

for 10 min before the hot plate was turned off and cooled down to room temperature. The sample was taken out of the tube and used for differential scanning calorimetry (*cf.* Section S4).

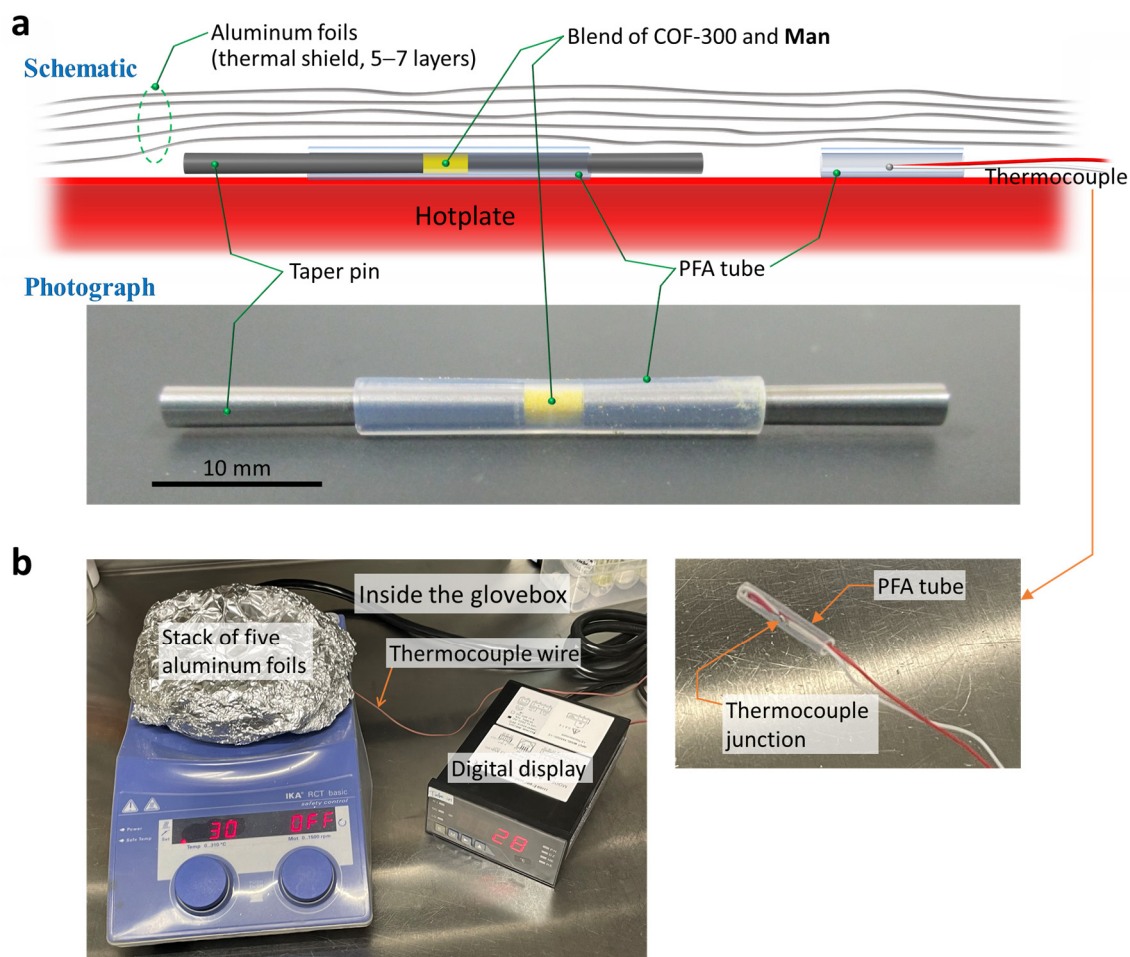


Fig. S2. Setup used for Method 2. (a) Schematic and photograph of the container, in which a blend of dried COF-300 crystals and **Man** in a PFA tube were confined and compressed horizontally by two steel taper pins. On the hotplate, a thermocouple enclosed in a PFA tube was also placed for accurate monitoring of the temperature. (b) Left: photograph of the entire setup placed in the glovebox. Right: photograph of the thermocouple enclosed in a PFA tube.

S2. Fundamental characterizations of COF-300 crystals

S2.1 Thermogravimetric analysis (TGA)

Fig. S3 shows the thermogravimetric analysis (TGA) profile of dried COF-300 crystals acquired under air flow using our TGA equipment (Thermo Plus EVO2, Rigaku). This result indicates high thermal stability of the COF-300 crystals.

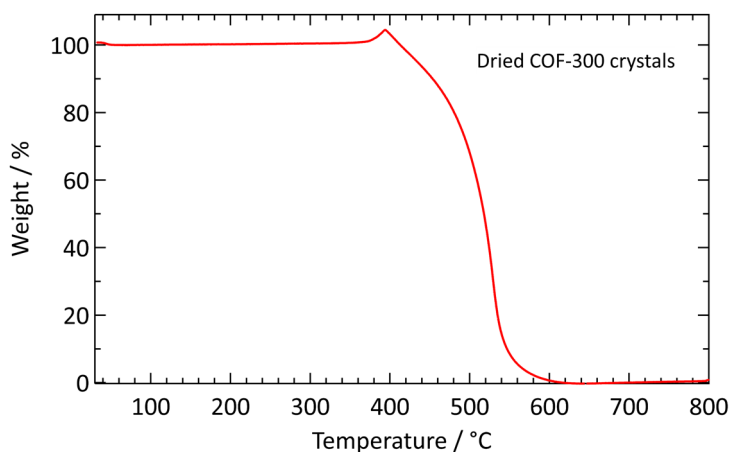


Fig. S3. TGA profile of dried COF-300 crystals, acquired at a heating rate of 5 °C min^{-1} and flowing 150 sccm of air. A slight increase in the mass just before the decomposition is attributed to oxidation of the framework.

S2.2 Specific heat measurements

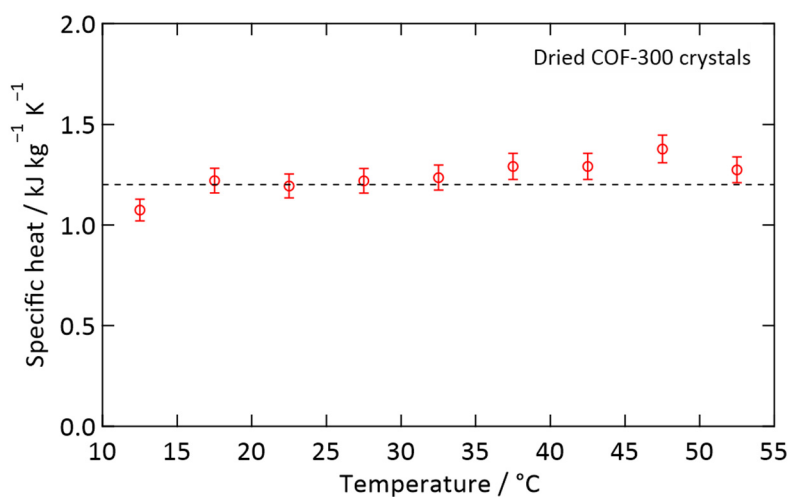


Fig. S4. Temperature dependence of the specific heat of dried COF-300 crystals, acquired by the stepwise method using sapphire as a reference. The dashed line indicates $1.2\text{ kJ kg}^{-1} \text{K}^{-1}$, which represents the specific heat close to room temperature.

Fig. S4 shows the specific heat of dried COF-300 crystals acquired under dry nitrogen gas flow using our power-compensation differential scanning calorimeter (DSC 8000, PerkinElmer) by the stepwise method^{S3} using sapphire as a reference. Each sample was crimped in an aluminium pan as described in Section S4. The specific heat close to room temperature was found to be *ca.* 1.2 kJ kg⁻¹ K⁻¹.

S2.3 Powder X-ray diffraction (PXRD) analysis

Powder X-ray diffraction (PXRD) measurements were conducted using an X-ray diffractometer (SmartLab, Rigaku). Figure S5 compares the PXRD patterns obtained from the “COF:Man (weight) = 1:1” sample, COF-300 crystals synthesised and post-treated according to the procedures described in Sections S1.2 and S1.3, respectively, and Man. See the caption for details.

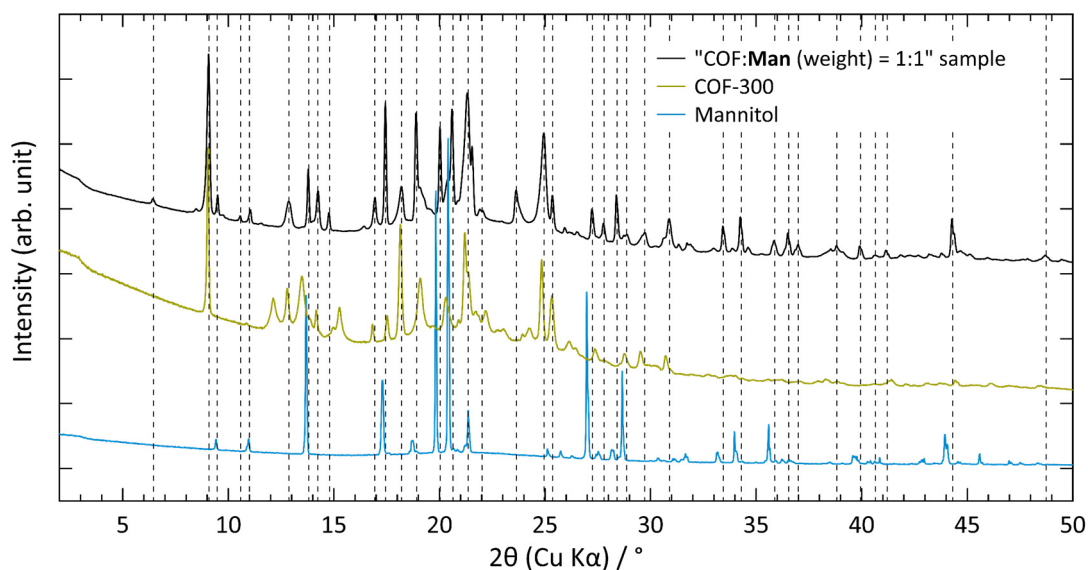


Fig. S5. Comparison of the PXRD patterns obtained from the “COF:Man (weight) = 1:1” sample (see Fig. 3 in the main text), COF-300 crystals we synthesised according to the method described in Section S1.2, and mannitol. The mannitol measured here was melted by heating to 175 °C, solidified by cooling to room temperature, and then ground into fine powder. Dashed lines indicate peaks appearing in the “COF:Man (weight) = 1:1” sample. See also the notes in the “Notes and references” section in the main text.

S2.4 Fourier-transform infrared (FT-IR) spectroscopy

The FT-IR spectrum of the COF-300 crystals is shown in Fig. S6 with those of the building-block molecules, **BDA** and **TAM** (*cf.* Fig. 1a in the main text). The spectra were acquired using a FT/IR-6100FV spectrometer (JASCO). The spectrum of the COF-300 indicates the complete consumption of the aldehyde (CHO-) and amine (NH₂-) moieties in the building-block molecules and the formation of imine (C=N) bonds.

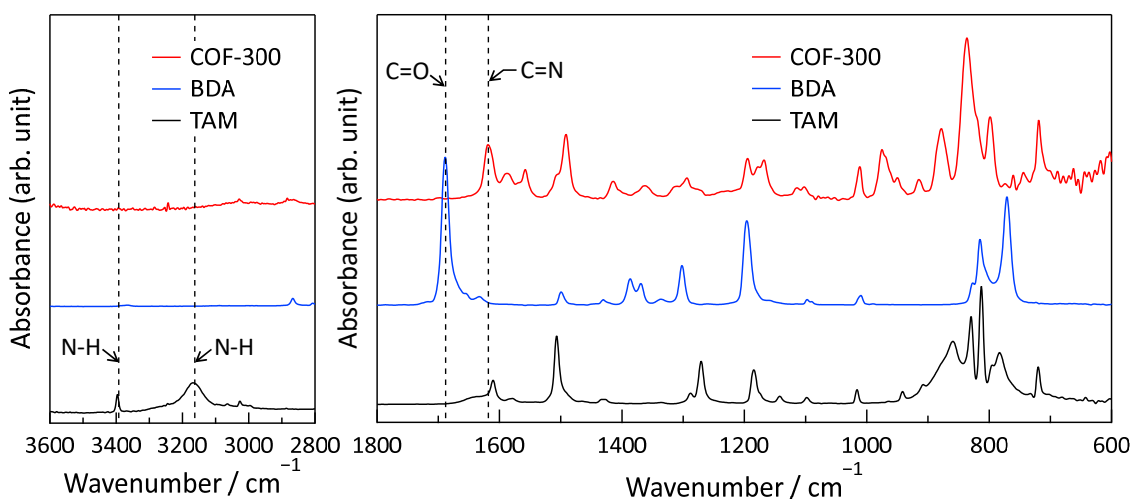


Fig. S6. FT-IR spectra of the COF-300 crystals compared with those of the building-block molecules used in this study.

S2.5 Nitrogen adsorption isotherms

The nitrogen (N₂) adsorption isotherms were measured on COF-300 crystals synthesised and post-treated by the present methods (see Sections S1.2 and S1.3, respectively) using a gas adsorption analyser (3Flex, Micromeritics). The results are shown in Fig. S7. The N₂ uptake was rather small, which is consistent with the results of our previous study^{S1} (see Section 8 of the ESI of ref. S1 for the pertinent discussions). Such a small uptake is ascribed to a contracted skeleton of COF-300 when no guest is included. (*cf.* Fig. S10a).

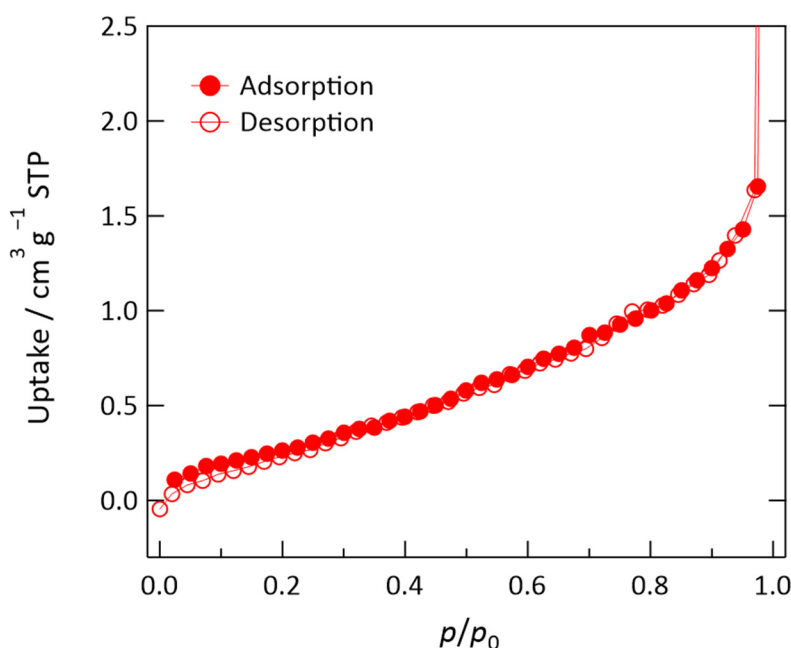


Fig. S7. N₂ gas adsorption isotherms of COF-300 prepared and post-treated according to the methods described in Sections S1.2 and S1.3, respectively.

S3. Single-crystal X-ray diffraction analysis

We conducted single-crystal X-ray diffraction (SXRD) measurements on COF-300 crystals filled with the maximal amount of **Eri** and **Man** (**Eri-COF** and **Man-COF**, respectively; see Fig. 2 in the main text) using a single-crystal X-ray diffractometer (XtaLAB Synergy, Rigaku). We used the SHELXT algorithm in Olex2[®] software for structural analysis, from which the amount of SA (*i.e.*, **Eri** or **Man**) impregnated in the pore of the COF was estimated. The results of the analyses are summarised in Tables S1 and S2 for the **Eri-COF** and **Man-COF** composites, respectively.

Figure S8 illustrates the result of the analysis performed on an **Eri-COF** composite crystal, in which the host framework of COF-300 is clearly seen. In addition, electrons of erythritol (brown dots) as guest molecules are seen in the pores of COF-300. The structure of **Eri-COF** was determined as an *I4₁/a* (No. 88) unit cell with $a = b = 26.3227 \text{ \AA}$, $c = 7.5857 \text{ \AA}$, $V = 5256.01 \text{ \AA}^3$. Crystal data and details of the structure refinement for **Eri-COF** are summarised in Table S1.

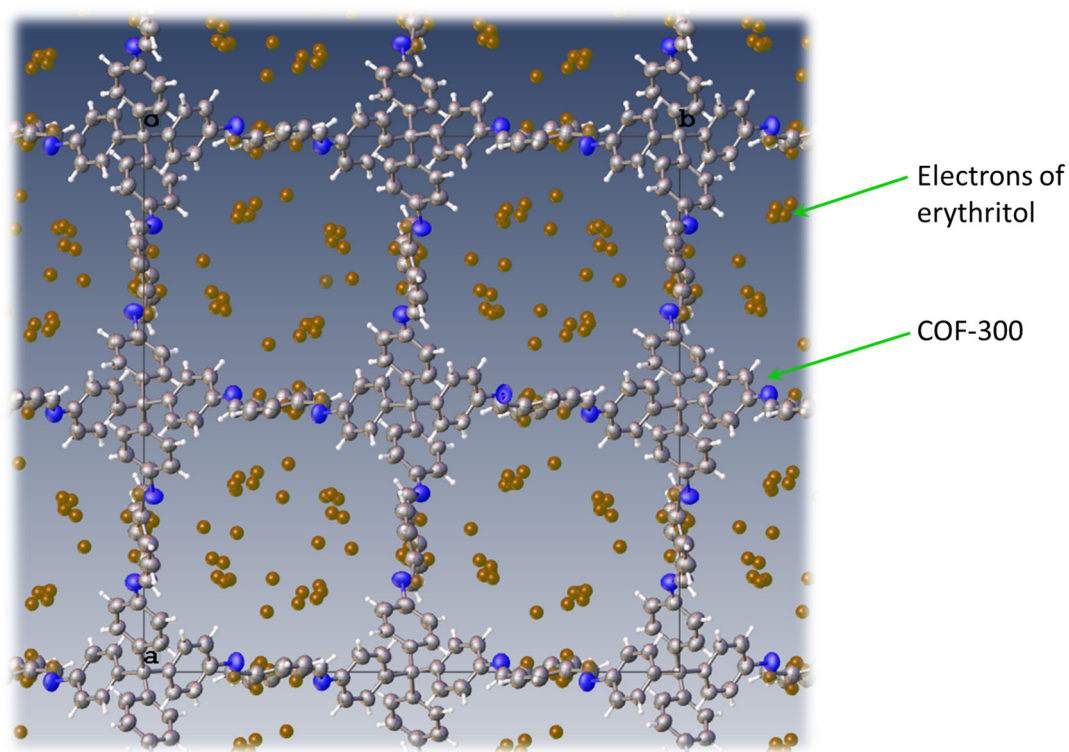


Fig. S8. Result of structural analysis on the SXRDR data obtained for an **Eri**-COF composite crystal, displayed by Olex2[®] software. See also Fig. S10. Brown dots in the voids of COF-300 skeleton represent electrons from **Eri** molecules, the atomic positions of which could not be determined due to the low translational and rotational symmetries of **Eri** molecules residing in the pores.

In SXRDR analysis, only molecules or moieties that have rigorous translational symmetry can appear with the exact shape in the reconstructed image. In COFs, interactions between guest molecules and the framework generally occur *via* van der Waals or hydrogen-bond interactions,^{S5} especially when both COF framework and guest species are charge-neutral, as in the present case. Because of this aspect, the translational symmetry of SA molecules residing along the 1D pore is not considered to be rigorous, and hence the shape of impregnated erythritol molecules in the pore does not appear exactly in Fig. S8. Thus, the erythritol molecules were found only as electron densities distributed over the pore, as represented by brown dots in Fig. S8.

The chemical composition of COF-300 is C₄₁H₂₈N₄ (formula mass: 576.67 g mol⁻¹).^{S5} Using the crystal structure determined by SXRDR, a solvent mask was applied onto the electrons residing in the pores of COF-300. Consequently, we found that approximately 13.7 erythritol molecules exist in the crystallographic unit cell of COF-300, which is

(C₄₁H₂₈N₄)₄ or C₁₆₄H₁₁₂N₁₆ with a formula mass of 576.67×4 = 2306.7 g mol⁻¹. Because the mass of **Eri** is 122.1 g mol⁻¹, we found that the mass ratio of **Eri**:COF at the maximal inclusion, R_{\max} , is

$$R_{\max} = \frac{122.1 \times 13.7}{2306.7} \approx 0.73$$

Therefore, we found that approximately 0.73 g of **Eri** can be impregnated into 1 g of dried COF-300. This corresponds to 0.73/(1 + 0.73) = 0.422... \cong 42 weight % loading in the composite. Furthermore, because the unit cell volume was found to be 5256 Å³ (Table S1), the density of this composite, ρ , is calculated to be

$$\rho \cong \frac{2306.7(1 + R_{\max})/N_A}{5256 \times 10^{-24}} \approx 1.26 \text{ g/cm}^3,$$

where N_A is the Avogadro constant and 10⁻²⁴ is a factor to convert Å³ into cm³.

Table S1. Crystal data, data collection, and structure refinement results for COF-300 constituting **Eri**-COF

Name	COF-300 constituting Eri -COF
Chemical composition	C ₁₆₄ H ₁₁₂ N ₁₆
Formula mass	2306.69
Crystal system	Tetragonal
Space group	<i>I</i> 4 ₁ / <i>a</i>
<i>a</i> , <i>b</i> , <i>c</i> , Å	26.3227(4), 26.3227(4), 7.58570(10)
α , β , γ , °	90, 90, 90
<i>V</i> , Å ³	5256.01(17)
<i>d</i> , g/cm ³	0.729
μ , mm ⁻¹	0.335
<i>Z</i>	1
Reflections collected	5393
Independent reflections	2394
2 θ_{\min} , °	6.716
2 θ_{\max} , °	150.116
<i>h</i> , <i>k</i> , <i>l</i>	-27 < <i>h</i> < 32, -31 < <i>k</i> < 12, -4 < <i>l</i> < 9
<i>R</i> int	0.0178
<i>R</i> ₁ [<i>F</i> ² > 2 σ (<i>F</i> ²)]	0.1485
<i>wR</i> ₂ (<i>F</i> ²)	0.4099
$\Delta\rho_{\max}$, e Å ⁻³	0.50
$\Delta\rho_{\min}$, e Å ⁻³	-0.54
Parameters	103
Restraints	0
GOF on <i>F</i> ²	1.835
Crystal size, mm ³	0.11 × 0.06 × 0.03
Radiation	Cu K α (λ = 1.54184 Å)
Temperature, K	223.15

Figure S9 illustrates the result of the analysis performed on a **Man**-COF composite crystal; the unit cell parameters were determined to be $a = 26.526 \text{ \AA}$, $b = 7.4416 \text{ \AA}$, $c = 26.974 \text{ \AA}$, and $V = 5320 \text{ \AA}^3$, with $P2$ (No.3) space group. However, because the “ R_{int} ” and “ R_1 ” factors were large (*cf.* Table S2), accurate determination of the framework of COF-300 was difficult using the SXRD data. Therefore, we constructed the structural model of the COF-300 constituting **Man**-COF using Materials Studio[®] software. The unit cell parameters and fractional coordinates of sp^3 carbon atoms in the TAM molecule obtained by our SXRD analysis were used for constructing the COF-300 structural model.

Similar to the case shown in Fig. S8, the electrons of mannitol molecules in the **Man**-COF composite crystal were seen as brown dots in the pores of COF-300 (Fig. S9). Although we could not accurately determine the structure of the COF-300 using the SXRD data, we have successfully determined the number of electrons existing in the pores of COF-300. Following similar procedures to those we applied to the **Eri**-COF

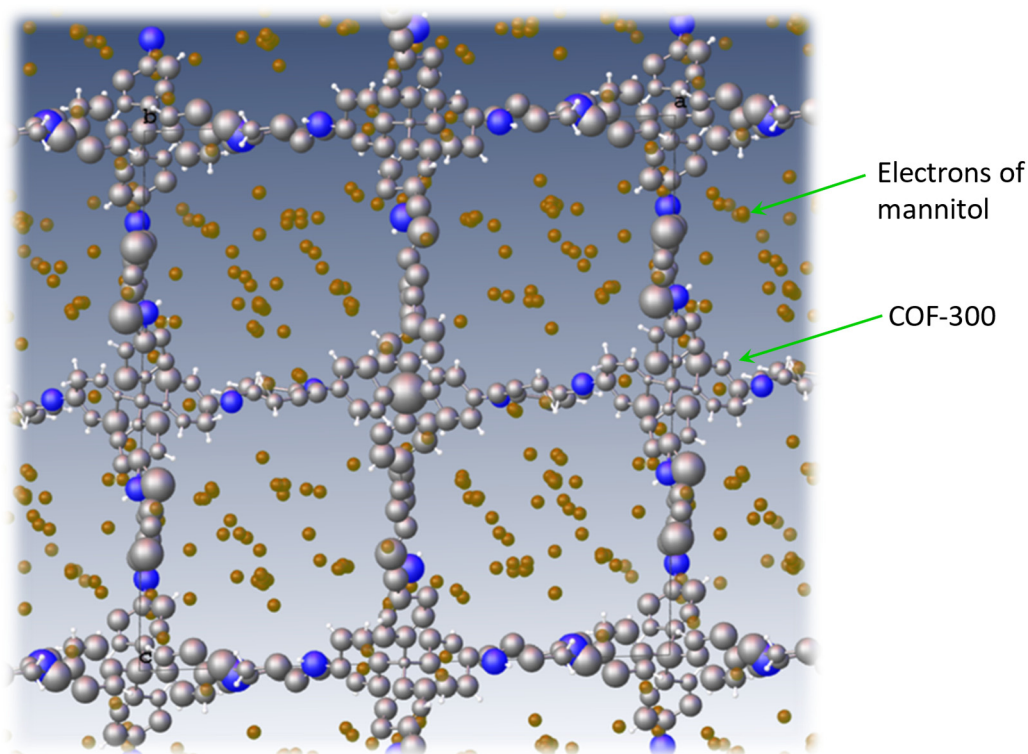


Fig. S9. Result of structural analysis on the SXRD data obtained for a **Man**-COF composite crystal, displayed by Olex2[®] software. See also Fig. S10. Brown dots in the voids of the COF-300 skeleton represent electrons from **Man** molecules, the atomic positions of which could not be determined due to the low translational and rotational symmetries of **Man** molecules residing in the pores, similar to the case shown in Fig. S8.

composite crystal above, we have determined R_{\max} , weight % loading at R_{\max} , and ρ to be *ca.* 0.77, $0.77/(1 + 0.77) = 0.435\dots \cong 44$ weight %, and 1.27 g/cm^3 , respectively, for a **Man**-COF composite crystal. The crystal data and details of the structural analysis are summarised in Table S2, in which the terms marked with an asterisk (*) were obtained from the aforementioned structural model constructed using Materials Studio[®] software.

Table S2. Crystal data, data collection, and structure refinement results for COF-300 constituting **Man**-COF

Name	COF-300 constituting Man -COF
Chemical composition	$\text{C}_{164}\text{H}_{112}\text{N}_{16}$ *
Formula mass	2306.69*
Crystal system	Monoclinic
Space group	$P2$
$a, b, c, \text{Å}$	26.526(7), 7.4416(5), 26.974(7)
$\alpha, \beta, \gamma, ^\circ$	90, 92.25(3), 90
$V, \text{Å}^3$	5320(2)
$d, \text{g/cm}^3$	0.72*
μ, mm^{-1}	0.327
Z	1*
Reflections collected	36662
Independent reflections	16115
$2\theta_{\min}, ^\circ$	4.582
$2\theta_{\max}, ^\circ$	155.704
h, k, l	$-32 \leq h \leq 33, -5 \leq k \leq 9, -34 \leq l \leq 33$
R int	0.3422
$R_1 [F^2 > 2\sigma(F^2)]$	0.1796
$wR_2 (F^2)$	0.4525
$\Delta\rho_{\max}, \text{e Å}^{-3}$	0.33
$\Delta\rho_{\min}, \text{e Å}^{-3}$	-0.56
Parameters	366
Restraints	1
GOF on F^2	1.048
Crystal size, mm^3	$0.11 \times 0.06 \times 0.03$
Radiation	Cu $K\alpha$ ($\lambda = 1.54184 \text{ Å}$)
Temperature, K	223.15

From these analyses, the numbers of **Eri** and **Man** molecules impregnated per $1 \mu\text{m}$ length of one pore of a COF-300 crystal have been found to be *ca.* 4,300 and 3,300 molecules μm^{-1} , respectively.

In Fig. S10 below, the frameworks of COF-300 saturated with **Eri** and **Man**, presented in Figs. S8 and S9, respectively, are compared with that of empty COF-300 previously determined from the data of rotation electron diffraction acquired in vacuum.^{S6} This comparison visually shows the change of the pore size caused by impregnation of the SA species into the COF pore.

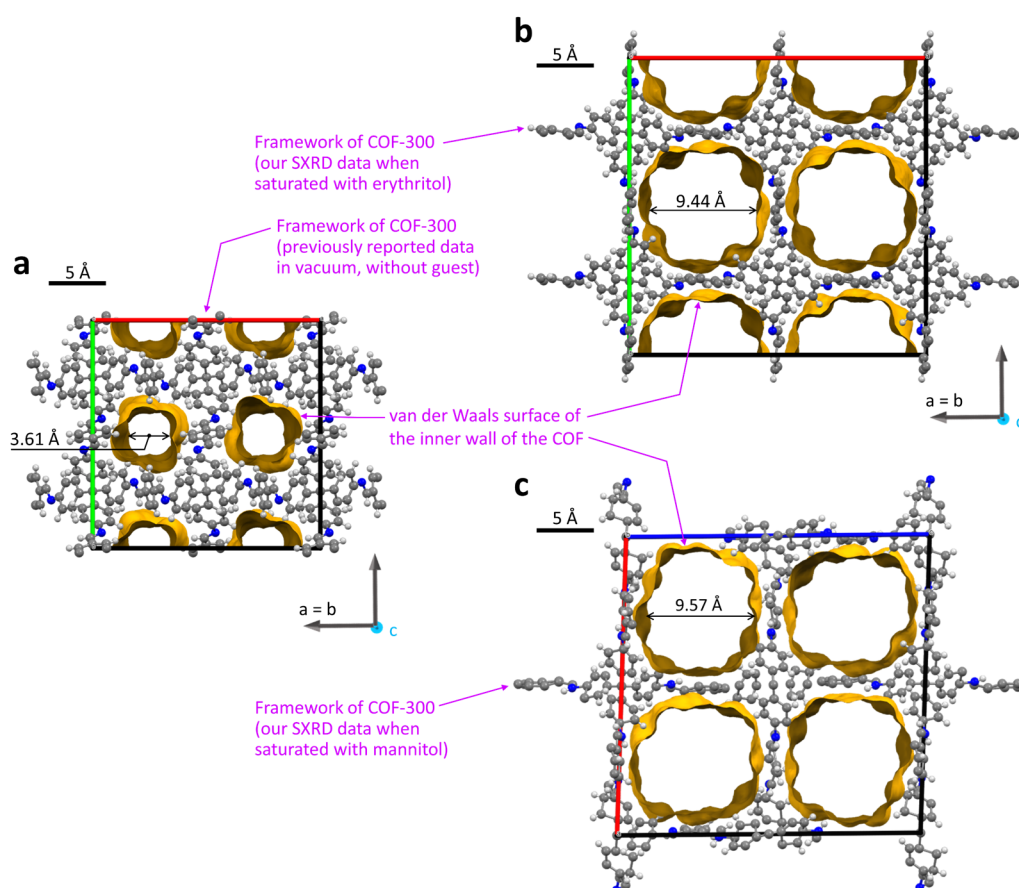


Fig. S10. Comparison of (a) the framework of empty COF-300 without guests, generated from the crystallographic data previously reported in ref. S6, (b) the framework of COF-300 saturated with **Eri** shown in Fig. S8, and (c) the framework of COF-300 saturated with **Man** shown in Fig. S9. These graphics were generated by Mercury[®] software.

S4. Differential scanning calorimetry (DSC)

Phase-change behaviours of the samples prepared by Method 2 were investigated by differential scanning calorimetry (DSC) using a power-compensation differential scanning calorimeter (DSC 8000, PerkinElmer). We enclosed our sample (typically 5–10 mg) in an aluminium pan using a crimper press to cover the pan. All weighing was performed with an ultra-micro balance (Cubis MSA2.7S-000-DM, Sartorius).

All measurements were performed at a scan rate of 2 °C/min with flowing dry nitrogen gas. Typically, the instrument was heated from 25 °C to 175 °C, at which point the temperature was held for 1 min, and then cooled down to 25 °C.

S5. Comparison of the molecular size of mannitol and pore size of COF-300

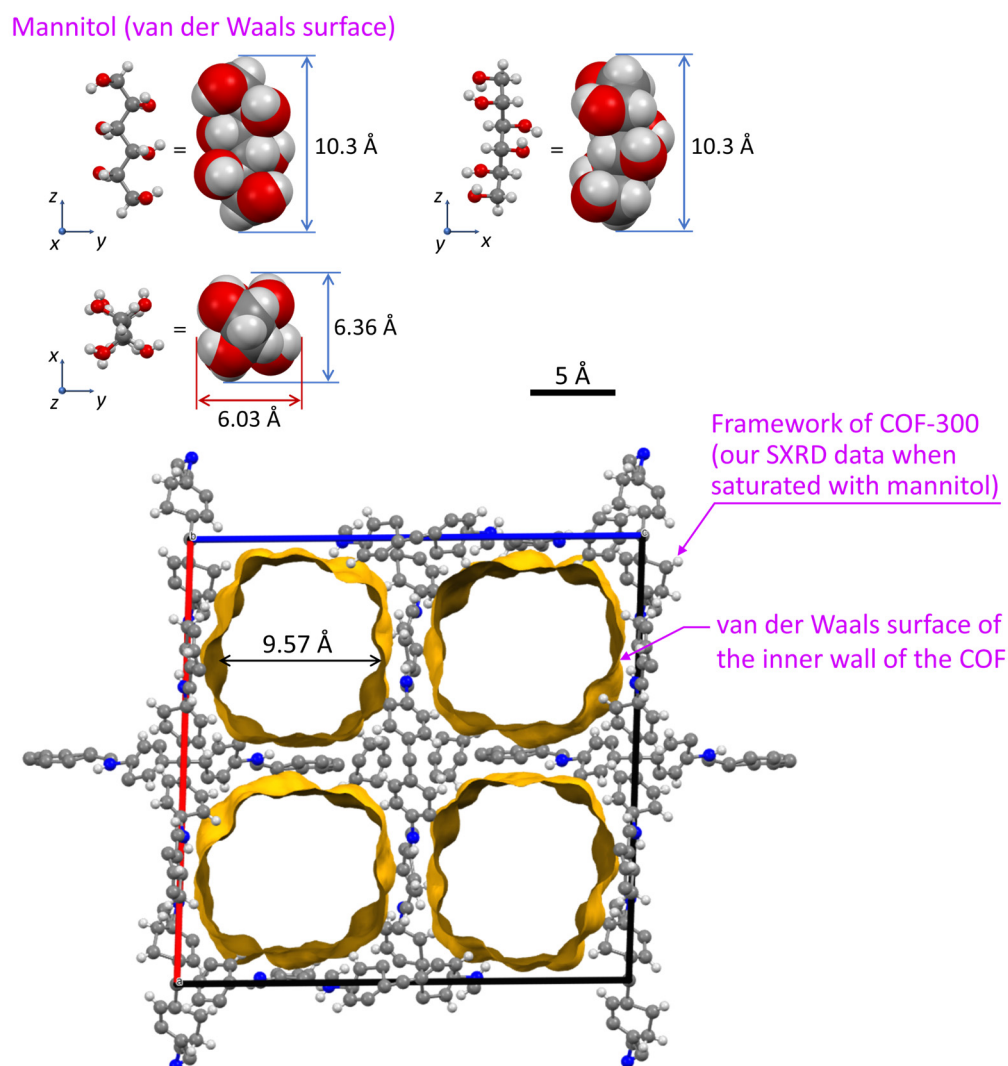


Fig. S11. Comparison of the molecular size of mannitol and the pore size of COF-300. The framework of COF-300 displayed here is the same as that shown in Fig. S9, which was determined by our SXRD analysis of a COF-300 crystal impregnated with the saturation amount of mannitol (*cf.* Fig. 2c in the main text). The scale bar (length: 5 Å) is common to all graphics, which were generated by Mercury[®] software.

S6. Number of hydrogen-bonded molecules to one Man molecule in crystal

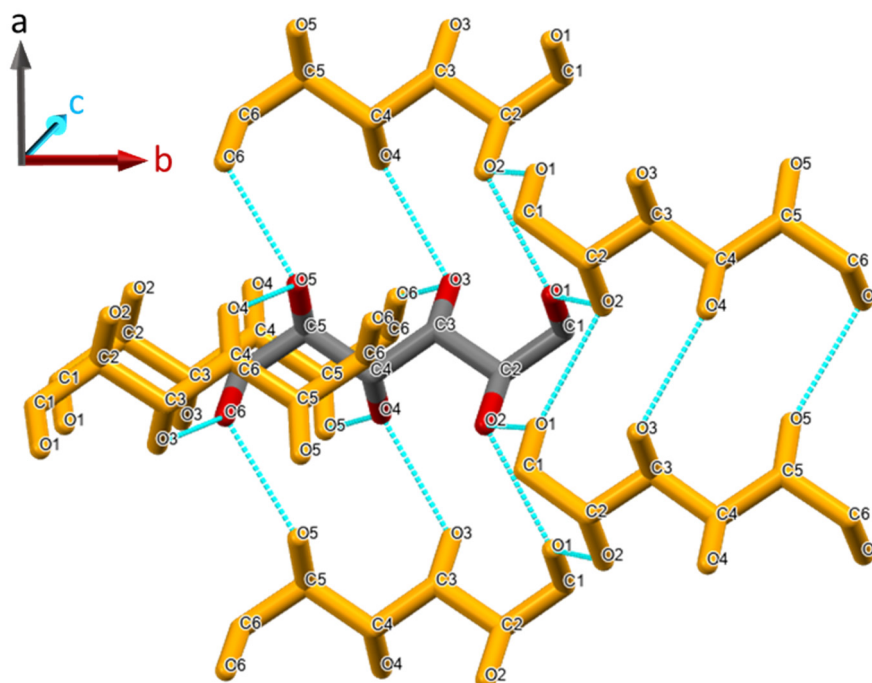


Fig. S12. The number of hydrogen-bonded molecules to one molecule in a β -D-mannitol crystal (structure reported by F. R. Fronczek et al., *Acta Cryst. C*, 2003, **59**, o567.), displayed using Mercury[®] software. Blue dotted lines represent hydrogen bonds. One mannitol molecule at the center (gray and red) interacts via hydrogen bonding with six surrounding mannitol molecules (orange).

S7. Temperature wave analysis (TWA)

The principle and details of the temperature wave analysis (TWA) and the microscale temperature wave analysis (μ -TWA) method have been compiled in the previous literature^{S7-S9} and the ISO standard.^{S10} The setup of the μ -TWA method used in this report is illustrated in Fig. 4a of the main text. First, under a stereomicroscope, a sample was placed on the ITO heater formed on a heater substrate. Next, a sensor substrate was placed on top, so that the sample was sandwiched by the ITO heater and the thermocouple junction (see Fig. 4a of the main text); their relative positions were precisely adjusted using vertical and lateral translational stages, which were driven by electric motors, while watching the digital images obtained using a stereomicroscope. Subsequently, the relative positions of these substrates were mechanically fixed *in situ* using UV curing resin

(NOA81, Norland Products) and then reinforced using epoxy resin so that interfacial contacts between the sample and the substrates were maintained during measurement. Next, power leads and thermocouple wires were bonded onto the substrates using silver paste; these junctions were protected by the UV resin. We determined the spacing between the substrates, which was the same as the sample thickness, from an average of spacing values measured by the optical interferometer for four positions around the sample. Finally, the cell was mounted in our home-built hot stage that has an optical window on the top; the sample being measured could be observed through the window using a polarized optical microscope. This hot stage was purged with nitrogen gas. The entire system is described in Fig. S13.

In measurements, a sinusoidal change in joule heating was posed to the ITO heater using a function generator (FG110, Yokogawa). The temperature wave propagated through the sample was detected by the thermocouple junction; see Ref. S6 for the principle and details of the TWA method. For the TWA measurements (Fig. 4d in the main text), the frequency of heating was scanned from 10 to 200 Hz and the thermal diffusivities were determined from the measured relationship between the frequency and the phase delay caused in the temperature wave on the sensor substrate.^{S7–S10} The temperature-dependent measurements (Fig. 4e in the main text) were conducted in the

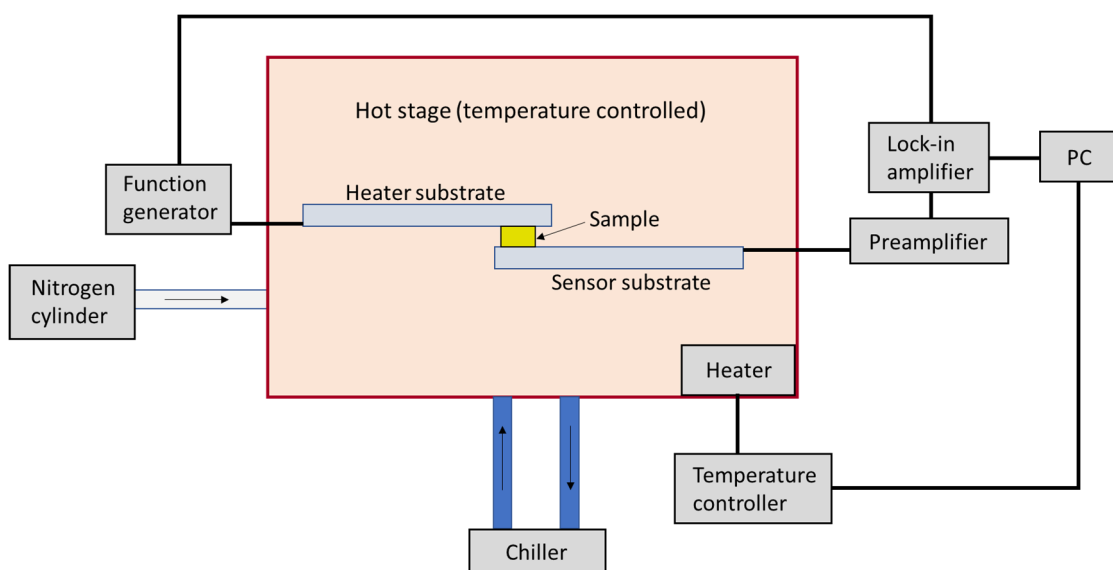


Fig. S13. Schematic diagram of the μ -TWA measurement system. The colored part is the measurement unit (home-built hot stage), which was placed under a stereomicroscope so that we could take photographs of the sample *in situ*. See also Figs. 4a and 4b in the main text.

‘side up’ configuration (*cf.* Fig. 4c in the main text) under a constant heating and cooling rate ($2\text{ }^{\circ}\text{C min}^{-1}$) with a 38-Hz temperature wave.

The periodic thermoelectric signal caused in the Au-Ni thermocouple deposited on the sensor substrate was led to a preamplifier (LI-75A, NF corporation) and then to a lock-in amplifier (SRS830, Stanford Research). The temperature of the hot stage was controlled by electric heating with a temperature controller and water circulation from a chiller, as illustrated in Fig. S13. The temperature at the sample position was calibrated using the melting points of **Man** (T_m : $167\text{ }^{\circ}\text{C}$) and liquid crystal 4-cyano-4'-pentylbiphenyl (5CB, T_m : $35\text{ }^{\circ}\text{C}$). The latter was purchased from TCI (purity: $> 98.0\%$). See footnote§§ in the main text for details of the temperature calibration.

In this study, we used two crystallographically equivalent sample configurations, ‘face up’ and ‘side up,’ as shown in Fig. 4c in the main text. Although they were physically equivalent experiments that yielded the same results (*cf.* the results for COF-300 crystals in Fig. 4d in the main text), we have recently been using the ‘side up’ configuration more frequently because we think it might result in better contact between the sample and the substrates.

Because of the necessity of forming good contacts between the sample and the substrates and owing to the shape of the COF-300 crystal (*cf.* Fig. 1a in the main text), our thermal diffusivity measurements in the present study were limited to detection along the a and b axes. In the future, we would be able to do measurements along the c axis, which would be more interesting as that axis corresponds to the direction of the one-dimensional pore of COF-300.

S8. *In situ* observations of a Man-COF crystal during experiment shown in Fig. 4e

During the experiment illustrated in Fig. 4e in the main text, we observed the fusion points of two **Man** droplets—one on the heater substrate and the other on the sensor substrate—with a polarizing microscope on the μ -TWA measurement system. The purpose of these observations is to calibrate the temperature of the sample *in situ* during the experiments; see footnote§§ in the main text for details of the temperature calibration.

Panel (a) of Fig. S14 shows the α - T curve for the second heating process in Fig. 4e of the main text. For the timings of (i), (ii), and (iii) in the heating process at $2\text{ }^{\circ}\text{C min}^{-1}$

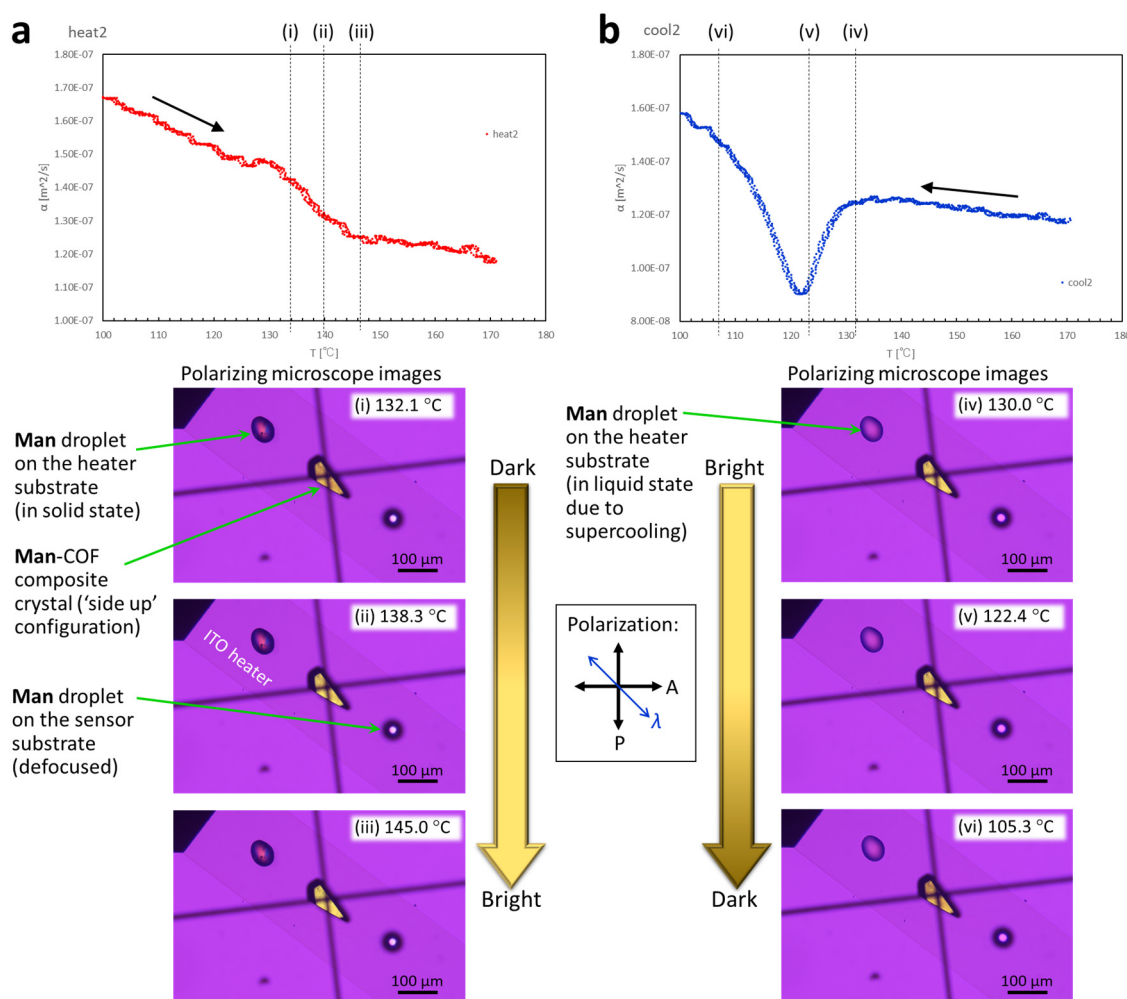


Fig. S14. *In situ* recorded snapshot images under a polarizing microscope during the (a) second heating and (b) second cooling processes shown in Fig. 4e in the main text. The thickness of the **Man**-COF composite crystal was 67.2 μm . The fusion points of two reference droplets of mannitol on the heater and sensor substrates were used to calibrate the temperature of this experiment. Apparent color changes occurred in the course of the processes (i) \rightarrow (iii) and (iv) \rightarrow (vi), for which the α - T curves in the panels (a) and (b) exhibited changes, respectively. The polarizing microscope observations were conducted under a crossed-Nicols configuration with a retardation plate of 530 nm.

indicated in the graph, where the temperatures at the sample position were 132.1, 138.3, and 145.0 $^{\circ}\text{C}$, respectively, the corresponding photographs of the sample area taken under the polarizing microscope are presented below the graph. As shown, from (i) to (iii), a clear change in the brightness (dark to bright) of the **Man**-COF composite crystal was observed. Similarly, as shown by panel (b), in which the α - T curve for the second cooling process in Fig. 4e of the main text is shown, a similar change in the brightness of the

crystal (bright to dark) was observed as the temperature descended from (iv) to (vi). These results support the conclusion that the changes exhibited by the α - T curves reflect real state transitions occurring in the **Man**-COF composite crystal.

See also *Supplementary Movies*, from which these snapshots were extracted.

Movie S1 (i) 132.1 °C: 0–1 s; (ii) 138.3 °C: 20–21 s; (iii) 145.0 °C: 43–44 s

Movie S2 (iv) 130.0 °C: 0–1 s; (v) 122.4 °C: 25–26 s; (vi) 105.3 °C: 86–87 s

References

- S1. X. Wang, R. Enomoto, and Y. Murakami, *Chem. Commun.*, 2021, **57**, 6656.
- S2. D. Zhu and R. Verduzco, *ACS Appl. Mater. Interfaces*, 2020, **12**, 33121.
- S3. See, for example, R. Pilar, P. Honcova, P. Kostal, G. Sadovska and L. Svoboda, *J. Therm. Anal. Calorim.*, 2014, **118**, 485.
- S4. H. Neumann, S. Niedermaier, S. Gschwander and P. Schossig, *Thermochim. Acta*, 2018, **660**, 134.
- S5. T. Ma, E. A. Kapustin, S. X. Yin, L. Liang, Z. Zhou, J. Niu, L. H. Li, Y. Wang, J. Su, J. Li, X. Wang, W. D. Wang, W. Wang, J. Sun and O. M. Yaghi, *Science*, 2018, **361**, 48.
- S6. T. Ma, J. Li, J. Niu, L. Zhang, A. S. Etman, C. Lin, D. Shi, P. Chen, L. H. Li, X. Du, J. Sun and W. Wang, *J. Am. Chem. Soc.*, 2018, **140**, 6763.
- S7. T. Hashimoto, J. Morikawa, T. Kurihara and T. Tsuji, *Thermochim. Acta*, 1997, **304-305**, 151.
- S8. A. Orie, J. Morikawa and T. Hashimoto, *Thermochim. Acta*, 2012, **532**, 148.
- S9. M. Ryu, S. Takamizawa and J. Morikawa, *Appl. Phys. Lett.*, 2021, **119**, 251902.
- S10. ISO 22007-3:2008. URL: <https://www.iso.org/standard/41063.html>